Evidence for a Proposed Intermediate Redox State in the CO/CO_2 Active Site of Acetyl-CoA Synthase (Carbon Monoxide Dehydrogenase) from *Clostridium thermoaceticum*†

Daniel M. Fraser‡ and Paul A. Lindahl*,§

Departments of Chemistry and of Biochemistry and Biophysics, Texas A&M University, College Station, Texas 77842

Received February 18, 1999; Revised Manuscript Received September 17, 1999

ABSTRACT: When samples of the enzyme in the C_{red1} state were reduced with Ti^{3+} citrate, the C-cluster stabilized in an EPR-silent state. Subsequent treatment with CO or dithionite yielded C_{red2}. The EPR-silent state formed within 1 min of adding Ti^{3+} citrate, while C_{red2} formed after 60 min. Ti^{3+} citrate appeared to slow the rate by which C_{red2} formed from C_{red1} and stabilize the C-cluster in the previously proposed C_{int} state. This is the first strong evidence for C_{int}, and it supports the catalytic mechanism that required its existence. This mechanism is analogous to those used by flavins and hydrogenases to convert between $n = 2$ and $n = 1$ processes. Ti^{3+} citrate had a different effect on enzyme in a CO_2 atmosphere; it shifted reduction potentials of metal centers (relative to those obtained using CO) and did not stabilize C_{int}. Different redox behavior was also observed when methyl viologen and benzyl viologen were used as reductants. This variability was exploited to prepare enzyme samples in which EPR from C_{red2} was present without interfering signals from B_{red}. The saturation properties of B_{red} depended upon the redox state of the enzyme. Three saturation "modes", called Sat1−Sat3, were observed. Sat1 was characterized by a sharp $g = 1.94$ resonance and low-intensity $g = 2.04$ and 1.90 resonances, and was observed in samples poised at slightly negative potentials. Sat2 was characterized by weak intensity from all three resonances, and was strictly associated with intermediate redox states and the presence of CO_2. Sat3 was characterized by strong broad resonances with normalized intensities essentially unchanged relative to nonsaturating conditions, and was observed at the most negative potentials. Each mode probably reflects different spatial relationships among magnetic components in the enzyme.

Nickel-containing carbon monoxide dehydrogenases (some of which are also acetyl-CoA synthases or decarbonylases) are found in numerous bacteria and archaea, including homoacetogens, methanogens, sulfate reducers, and some photosynthesizers (*1*−*4*). These enzymes catalyze the reversible reaction $CO + H_2O \rightleftharpoons CO_2 + 2e^- + 2H^+$.

Two metal−sulfur clusters in these enzymes, called B and C, are responsible for this activity (*5*−*8*). The C-cluster in the active site consists of a Ni−X−Fe_4S_4 cluster (where X is an unknown ligand). The oxidized C_{ox}[1] state corresponds to the Ni^{2+}−X−$[Fe_4S_4]^{2+}$ electronic configuration (*9*, *10*). It can be reduced by one electron ($E° = -0.15$ V vs NHE under CO_2 at pH 7) to the C_{red1} state (*11*). This $S = {}^1/_2$ state has the electronic configuration Ni^{2+}−X−$[Fe_4S_4]^{1+}$ and exhibits an EPR signal with g values of 2.01, 1.80, and 1.64 ($g_{av} = 1.82$) (*10*, *12*). The Ni^{2+} is at most weakly coupled to the cube. The Fe bridged to the Ni is probably five- or six-coordinate, including a hydroxyl group that may function in catalysis (*10*, *13*). As potentials are lowered further ($E° = -0.39$ V under CO_2 at pH 7), C_{red1} disappears and another $S = {}^1/_2$ state called C_{red2} appears (*12*, *14*). The electronic configuration of C_{red2} has not been established, but the associated EPR signal, with g values of 1.97, 1.87, and 1.75 ($g_{av} = 1.86$), is quite similar to that exhibited by C_{red1}, suggesting that the Fe_4S_4 cube remains in the 1+ core state. Anderson and Lindahl (*8*) proposed that C_{red2} is two electrons more reduced than C_{red1}, with one of the electrons localized on the Ni (affording Ni^{1+}) and the other reducing a hypothetical redox-active ligand to the Ni (called L_{red}). Thus, the electronic configuration of C_{red2} would be L_{red}−Ni^{1+}−X−$[Fe_4S_4]^{1+}$, while C_{red1} would have L oxidized. The hydroxyl group is not bound in C_{red2} (*13*).

C_{red1} and C_{red2} probably play important roles in catalysis (*5*−*14*). CO is proposed to bind the Ni^{2+} of C_{red1} and be attacked by the hydroxyl group bound at the bridging Fe.

† This research was supported by the National Institutes of Health (GM46441) and the Robert A. Welch Foundation (A1170).

* To whom correspondence should be addressed. Telephone: (409) 845-0956. E-mail: Lindahl@chemvx.tamu.edu.

‡ Department of Chemistry.

§ Departments of Chemistry and of Biochemistry and Biophysics.

[1] Abbreviations: EPR, electron paramagnetic resonance; ACS, acetyl-CoA synthase (previously carbon monoxide dehydrogenase, abbreviated CODH); Ti/Ar, Ti^{3+} citrate titration performed under Ar; Ti/CO_2, same as Ti/Ar but performed under CO_2; CO/Ar, CO titration performed under Ar; CO/CO_2, same as CO/Ar but performed under CO_2; MV/Ar, electrochemically reduced methyl viologen titration under Ar; MV/CO_2, same as MV/Ar but performed under CO_2; BV/CO_2, benzyl viologen titration performed under CO_2; Sat1−Sat3, three saturation modes for the B_{red} state; C_{ox}, C_{red1}, C_{int}, and C_{red2}, four redox states of the C-cluster, with C_{ox} fully oxidized and each subsequent state more reduced by one electron. Reduction potentials differ according to whether samples were under Ar or CO_2 (*14*), and this will be indicated by (CO_2) or (Ar) following the $E°$. Potentials are relative to the normal hydrogen electrode at pH 7.0 unless stated otherwise.

10.1021/bi990398f CCC: $18.00
Published on Web 11/05/1999

An unidentified base removes the proton from the resulting Ni-bound carboxylate, triggering decarboxylation and two-electron reduction of C_{red1} (yielding C_{red2}). In the reverse direction, CO_2 binds and oxidizes C_{red2}. Subsequent protonation and transfer of a hydroxyl group (to the Fe) yields CO bound to the Ni^{2+} of C_{red1} (*13*).

The B-cluster is an $[Fe_4S_4]^{2+/1+}$ cube that is diamagnetic when oxidized (B_{ox}) and exhibits a $g_{av} = 1.94$ signal when reduced ($E° = -0.41$ V under CO_2 at pH 7) to its $S = {}^1/_2$ B_{red} state (*9*, *10*, *12*, *14*). The B-cluster transfers electrons to and from the C-cluster and external $n = 1$ redox agents such as methyl viologen (MV) and Ti^{3+} citrate.

One puzzling aspect of the catalytic mechanism is that the B cluster is an $n = 1$ redox agent while the C cluster catalyzes an $n = 2$ redox process. Anderson and Lindahl suggested that the C-cluster must be stable in a redox state one electron more reduced than C_{red1} and one electron more oxidized than C_{red2} (*8*). This intermediate redox state, designated C_{int}, would be either $S = 0$ (or an integer), and probably EPR-silent. Thus, the absence of an EPR signal from reduced C-clusters would be evidence for C_{int}.

In this paper, we report the first substantial evidence for this hypothetical C_{int} state, and thus support for the proposed catalytic mechanism. Evidence was obtained by titrating the enzyme (ACS) from *Clostridium thermoaceticum* with various $n = 1$ reductants under Ar and CO_2 atmospheres and monitoring for a reduced EPR-silent state of the C-cluster. We also report subtle changes in the saturation properties of B_{red}, and further evidence for reductant-and-oxidant-dependent changes in the redox properties of the ACS clusters. These changes may reflect different protein conformations that allow the enzyme to operate reversibly over a wide range of CO/CO_2 pressures.

EXPERIMENTAL PROCEDURES

C. thermoaceticum cells were grown, and three batches of ACS were purified and assayed as described previously (*15*). Batches 1−3 had CO oxidation activities of 340, 240, and 320 units/mg, and CO/acetyl-CoA exchange activities of 0.21, 0.18, and 0.26 units/mg, respectively. Each batch was >90% pure as determined by visual inspection of SDS−polyacrylamide electrophoretic gels. Samples were purified, manipulated, and titrated in a glovebox (Vacuum/Atmospheres HE-453) containing an Ar atmosphere with <1 ppm O_2 (monitored by a Teledyne model 310 analyzer). Protein concentrations were determined by the Biuret method (*16*). The molecular mass of each $\alpha\beta$ dimeric unit is 154 700 Da (*17*). EPR spectra were recorded and analyzed as described previously (*18*, *19*).

Five titrations were performed as follows. Enzyme samples were concentrated using a 30 kDa Centricon concentrator (Amicon) and freed from dithionite by passage through a Sephadex G-25 (1.5 cm × 15 cm) column equilibrated in buffer. The buffer used in the titration with Ti^{3+} citrate under Ar (designated Ti/Ar) was 50 mM Tris (pH 8.0), while that used in all other titrations was 50 mM MES (pH 6.3). Protein concentrations were determined, and samples were diluted with buffer to 4.0 mg/mL (except where noted). Buffers were degassed on a Schlenk line, and then left overnight in the glovebox prior to use for removal of residual O_2. Research grade CO and CO_2 were O_2-scrubbed (Oxisorb, MG Scientific) prior to use. All other chemicals were used without further purification.

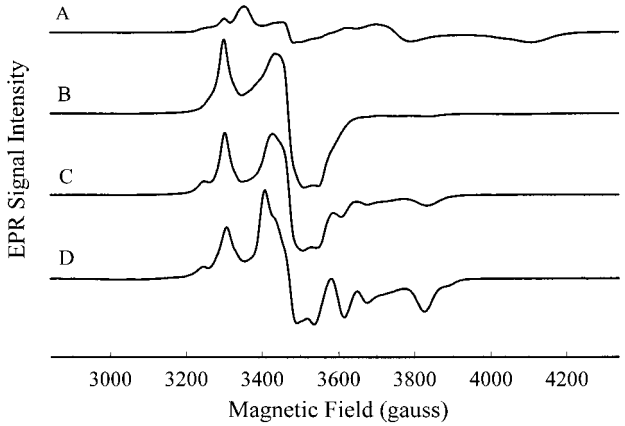

FIGURE 1: EPR of ACS reduced by Ti^{3+} citrate under Ar: (A) reductant-free ACS, (B) same as for part A with 9 equiv/$\alpha\beta$ of Ti^{3+} citrate, (C) same as for part B with 1 atm of CO, and (D) ACS (batch 3) reduced with 5 equiv/$\alpha\beta$ of Ti^{3+} citrate in 1 atm of CO_2. EPR conditions were as follows: microwave frequency, 9.42 GHz; temperature, 10 K; modulation amplitude, 11.8 G; modulation frequency, 100 kHz; and microwave power, 20 mW.

Ti^{3+} Citrate Titrations. Ti^{3+} citrate was prepared (*20*) using $TiCl_3$ (Sigma) immediately prior to the experiment. Its concentration was determined by UV−vis spectroscopy assuming an ϵ_{340} of 0.73 mM^{-1} cm^{-1}, and then adjusted to 11 mM with buffer. For the titration performed under Ar, designated Ti/Ar, the enzyme (batch 1) was transferred to EPR tubes containing increasing amounts of Ti^{3+} citrate (final ACS concentration of 10 mg/mL). Resulting solutions were mixed for 1 min and then frozen in liquid N_2. Procedures used for the Ti^{3+} citrate titration under CO_2 (designated Ti/CO_2) were the same as those for the methyl viologen (MV) titration (MV/CO_2) (see below) except that the Ti^{3+} citrate was diluted to 2 mM and the protein concentration (batch 3) was 4.0 mg/mL. The titration was simulated using the best-fit PMX parameters for titration 2 (*11*).

Titrations with Methyl Viologen and Benzyl Viologen (BV). For the MV titrations, half of the reductant-free enzyme (batch 2) was incubated under CO_2 for 45 min (MV/CO_2), while the other half was incubated under Ar (MV/Ar). Aliquots were then transferred to modified EPR cuvettes as described in refs *11* and *21*, combined with increasing amounts of reduced viologen, mixed for 1 min, incubated for an additional 1 min, and then frozen by rapid immersion in liquid N_2-cooled isopentane. The BV titration under CO_2 (BV/CO_2) was performed equivalently (also using batch 2). Viologens were reduced in 50 mM MES (pH 6.3), 5% (v/v) ethanol, and 200 mM KCl using a three-electrode system as described previously (*22*). The final concentrations of the reduced MV and BV, determined before and after the titrations, were 0.91 ($\epsilon_{604} = 13.9$ mM^{-1} cm^{-1}) and 0.85 mM ($\epsilon_{578} = 8.65$ mM^{-1} cm^{-1}), respectively.

RESULTS

Titration of ACS under an Ar Atmosphere with Ti^{3+} Citrate. When we reduced a sample of ACS in the C_{red1} state (Figure 1A) with Ti^{3+} citrate and then rapidly froze it, the $g_{av} = 1.82$ signal, which characterizes that state, disappeared, but the $g_{av} = 1.86$ signal, which characterizes the C_{red2} state, did not appear (Figure 1B). This is unprecedented behavior

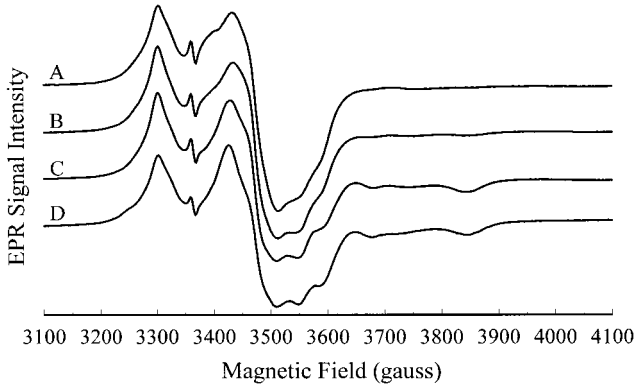

FIGURE 2: EPR of ACS reduced by Ti^{3+} citrate/Ar and frozen at different times: (A) ACS reduced with 10 equiv/$\alpha\beta$ of Ti^{3+} citrate in Ar, frozen after incubation for 1 min, (B) same as for part A but frozen after 5 min, (C) same as for part A but frozen after 60 min, and (D) same as for part A after anaerobic thawing and addition of 10 mM sodium dithionite. EPR conditions are the same as described in the legend of Figure 1. The EPR signal from Ti^{3+} citrate contributes to the region of the $g_{av} = 1.94$ signal of ACS, but it is largely saturated under the conditions that are employed.

because a similar treatment using other low-potential reductants (CO and dithionite) yields the C_{red2} state.

One intriguing possibility is that Ti^{3+} citrate reduced the C-cluster to the hypothetical EPR-silent C_{int} state. However, other possibilities must also be considered. For example, Ti^{3+} citrate may have destroyed the C-cluster. However, subsequent treatment of Ti^{3+} citrate-reduced samples with CO (Figure 1C) or dithionite (not shown) yielded the C_{red2} state. Thus, the C-cluster must have remained functional and undamaged in the EPR-silent state generated by treatment with Ti^{3+} citrate.

Another possibility was that Ti^{3+} citrate oxidized the C-cluster to the C_{ox} state. This is counterintuitive since Ti^{3+} citrate is a powerful reductant [$E^{\circ\prime} = -0.48$ V (*20*)], not an oxidant. It also seems unlikely because subsequent addition of the oxidant CO_2 to Ti^{3+} citrate-treated samples yielded the C_{red2} state (Figure 1D). However, neither result strictly excludes this possibility, because redox agents are known to alter the properties of the C-cluster (see below), and it would be possible to rationalize these results by invoking such effects.

However, this possibility was further discounted by treating ACS samples in the C_{red1} state with Ti^{3+} citrate and then freezing them at different times. The sample incubated for 1 min showed full conversion to the EPR-silent state (Figure 2A). That incubated for 5 min exhibited similar features except that a hint of the C_{red2} state was evident (Figure 2B). The sample incubated for 60 min exhibited the C_{red2} state (Figure 2C) virtually identical to that obtained by adding dithionite to the sample used to generate Figure 2A (Figure 2D). This demonstrates that Ti^{3+} citrate is powerful enough to reduce the C-cluster to the C_{red2} state, and that it acts by slowing the rate by which C_{red2} is formed from C_{red1}. This excludes the possibility that the EPR-silent state generated by treatment with Ti^{3+} citrate was C_{ox} (because it seems unreasonable to suggest that Ti^{3+} citrate first oxidized C_{red1} to C_{ox} and then reduced C_{ox} to C_{red2}).

Another possibility was that Ti^{3+} citrate rapidly reduced C_{red1} to an EPR-silent state one electron more reduced than C_{red2}. Accordingly, the slow development of C_{red2} would

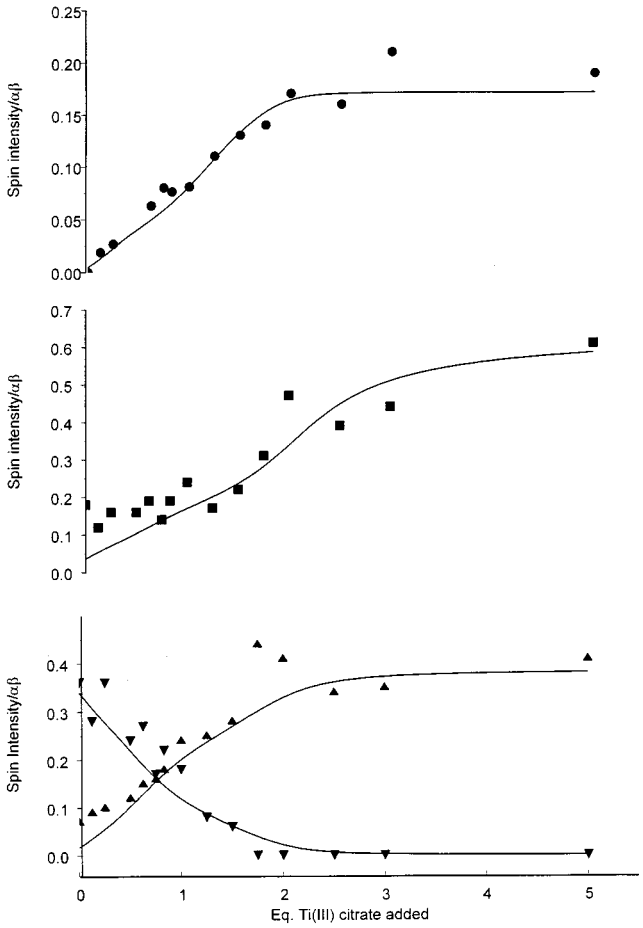

FIGURE 3: Curves and simulation for the titration of ACS with Ti^{3+} citrate under CO_2: (●) NiFeC signal (A_{red}−CO state), (■) $g_{av} = 1.94$ signal (B_{red}), (▼) $g_{av} = 1.82$ signal (C_{red1}), and (▲) $g_{av} = 1.86$ signal (C_{red2}). Solid lines are simulations performed as described previously (*14*) using the best-fit parameters for titration 2, the PMX model, except that EQ_{init} was 0.5 equiv/$\alpha\beta$, $E^{\circ\prime}_{A_{ox}/A_{red}-CO}$ was −0.130 V, $E^{\circ\prime}_{B_{ox}/B_{red}}$ was −0.391 V, $E^{\circ\prime}_{C_{red1}/C_{int}}$ was −0.375 V, and $E^{\circ\prime}_{C_{int}/C_{red2}}$ was −0.335 V. $E^{\circ\prime}_{CO/CO_2}$ was switched to −0.440 V, to estimate the potential for Ti^{3+} citrate at pH 6.3 (*20*).

reflect the slow oxidation of this state to C_{red2}. However, we discount this possibility because subsequent addition of reductants with potentials comparable to that of Ti^{3+} citrate (i.e., dithionite or CO) causes rapid formation of C_{red2}, and it seems unreasonable to suggest that these reductants oxidized the enzyme. We conclude that the EPR-silent state obtained by Ti^{3+} citrate is C_{int}, and propose that Ti^{3+} citrate reduces C_{red1} to C_{int} rapidly, but reduces C_{int} to C_{red2} more slowly. In contrast, dithionite appears to reduce C_{red1} to C_{int} slowly and C_{int} to C_{red2} rapidly (*8*). The substrates CO and CO_2/dithionite increase these rates substantially (*8*). Thus, the rate by which the C-cluster can be reduced critically depends on the reductant and/or atmosphere employed.

Titration of ACS under a CO_2 Atmosphere with Ti^{3+} Citrate. Another sample of ACS in a CO_2 atmosphere was exposed to increasing amounts of Ti^{3+} citrate. The sample lacking Ti^{3+} citrate exhibited $g_{av} = 1.82$, 1.86, and 1.94 signals, all at low intensities [the C_{red1}/C_{red2} and B_{ox}/B_{red} couples have similar $E^{\circ\prime}$ values under CO_2 (*14*)]. With increasing amounts of Ti^{3+} citrate, the A_{red}−CO state started to develop immediately (Figure 3, top plot), while the C_{red1}/C_{red2} crossover point occurred nearly 0.5 equiv/$\alpha\beta$ later than predicted by simulations using the best-fit parameters for

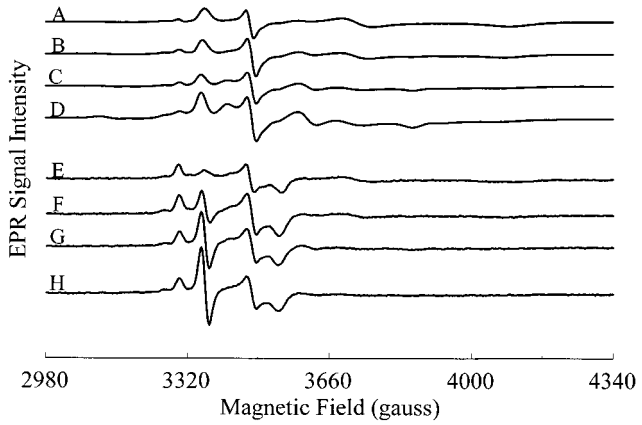

FIGURE 4: EPR of ACS titrated with methyl viologen under argon. Reductant-free ACS and the following amounts of reduced methyl viologen (in equivalents per $\alpha\beta$): (A) 0.0, (B) 0.5, (C) 1.5, and (D) 2.0. EPR conditions as described in the legend of Figure 1. E−H, same as parts A−D, respectively, except that the microwave power was 0.05 mW.

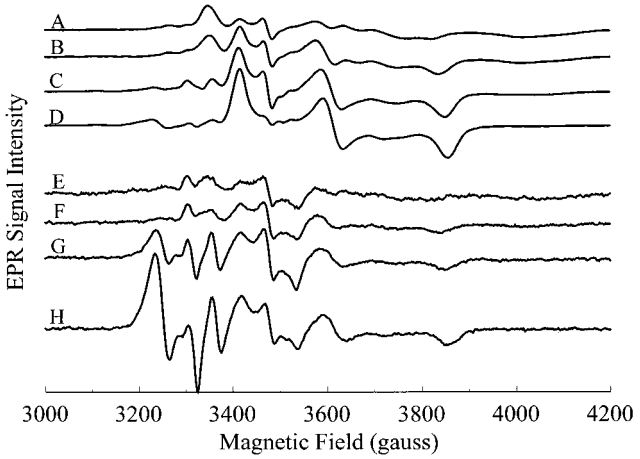

FIGURE 5: EPR of ACS titrated with methyl viologen under CO_2. Reductant-free ACS with the following amounts of reduced methyl viologen (in equivalents per $\alpha\beta$): (A) 0.0, (B) 0.38, (C) 1.25, and (D) 2.0. EPR conditions as described in the legend of Figure 1. E−H, same as parts A−D, respectively, except that the microwave power was 0.05 mW.

our CO/CO_2 titrations (Figure 3, bottom plot). Best-fit simulation of the Ti/CO_2 titration required the $E°$ (CO_2, pH 6.3) values given in the Figure 3 legend. Relative to CO, Ti^{3+} citrate in the presence of CO_2 increased the reduction potentials of the A_{ox}/A_{red}−CO and C_{int}/C_{red2} couples by 0.03 and 0.01 V, respectively, and decreased those for the B_{ox}/B_{red} and C_{red1}/C_{int} couples by 0.03 and 0.04 V, respectively. This titration reveals that the redox potentials of the ACS clusters vary depending on the reductants and the atmosphere used.

Titrations of ACS under Ar and CO_2 Atmospheres with Methyl Viologen. This sensitivity of cluster properties to the presence of redox agents is further illustrated by titrations performed with electrochemically reduced methyl viologen under Ar and CO_2 atmospheres. MV^{1+} is a milder $n = 1$ reductant than Ti^{3+} citrate [$E°_{MV^{2+}/MV^{1+}} = -0.44$ V (*23*)]. Reductant-free ACS under Ar exhibited the B_{red} and C_{red1} states (Figure 4A,E). As MV^{1+} was added, some but not all of the C_{red1} converted to C_{red2} (Figure 4B−D). The matched reductant-free samples under CO_2 exhibited EPR signals from B_{red}, C_{red1}, and C_{red2} (Figure 5A,E). However, increasing the level of MV^{1+} caused the intensity of C_{red1} to decline and that of C_{red2} to develop fully (Figure 5B−D). This full development suggests that $E°_{C_{red1}/C_{red2}}$ was less negative in MV/CO_2 than in MV/Ar, and was similar to that observed in CO/CO_2 and Ti/CO_2 titrations (about −0.34 V). Interestingly, MV^{1+} did not reduce B_{ox} (the $g_{av} = 1.94$ signal intensities at the beginning and end of the titration were similar) (Figure 5E−H). This suggests that $E°_{B_{ox}/B_{red}}$ in MV/CO_2 was more negative than in CO/CO_2 (−0.37 V), where both B_{red} and C_{red2} developed at nearly the same potential (*11*). $E°_{B_{ox}/B_{red}}$ is probably more similar to that in Ti/CO_2 (−0.39 V), where C_{red1} converted to C_{red2} at more positive potentials that B_{ox} was reduced (Figure 3, middle panel vs lower panel). Thus, under CO_2, MV^{1+} was not sufficiently powerful to reduce the B_{ox} cluster fully but was sufficiently powerful to reduce C_{red1} to C_{red2}. The 20 mW spectrum (Figure 5D) essentially consisted of only the $g_{av} = 1.86$ signal from C_{red2}. This is the first sample of ACS in which the $g_{av} = 1.86$ signal is present without other "interfering" EPR signals. At low power, a small amount of the $g_{av} = 1.94$ signal was evident (0.1 spin/$\alpha\beta$, or ∼15% of fully reduced), as well as the NiFeC signal (Figure 5H).

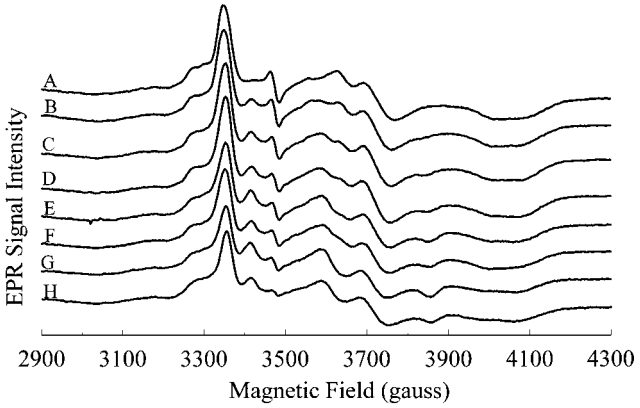

FIGURE 6: EPR of ACS titrated with benzyl viologen under CO_2. Reductant-free ACS with the following amounts of reduced benzyl viologen (in equivalents per $\alpha\beta$): (A) 0.0, (B) 0.2, (C) 0.4, (D) 0.7, (E) 0.9, (F) 1.25, (G) 2.0, and (H) 5.0. EPR conditions as described in the legend of Figure 1.

Although not as obvious as with Ti/Ar, the MV/Ar and MV/CO_2 titrations also provided evidence for the C_{int} state. At the end of the MV/Ar titration, spectra exhibited only ∼0.15 spin/$\alpha\beta$ of C-cluster signals (C_{red1} plus C_{red2}). In contrast, by the end of the MV/CO_2 titration, the C-cluster signal (exclusively C_{red2}) quantified to 0.4 spin/$\alpha\beta$. Since these were matched samples (the same sample divided into two aliquots), comparing their relative intensities is reliable. Such a comparison suggests that ∼60% of the redox-active C-clusters were in an EPR-silent state (i.e., C_{int}) at the end of the MV/Ar titration.

Titration of ACS under a CO_2 Atmosphere with Benzyl Viologen. The effect of BV/CO_2 was similar to that of MV/CO_2, except that BV is a milder reductant [$E°_{BV^{1+}/BV^{2+}} = -0.35$ V (*24*)], and so the resulting samples were not as reduced. The reductant-free sample for the BV/CO_2 titration (Figure 6A) was slightly more oxidized than that for the MV/CO_2 titration (Figure 5A), and the final BV/CO_2 sample (Figure 6H) was slightly more reduced than the MV/CO_2 sample used to generate Figure 5A. Thus, the BV/CO_2

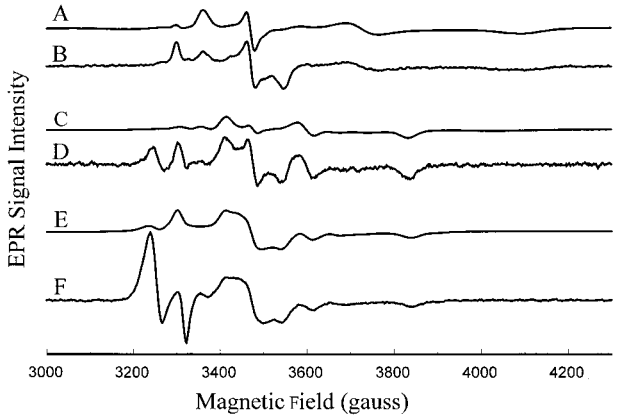

FIGURE 7: B_{red} saturation patterns. A and B, same as parts A and E of Figure 4, respectively; C, ACS reduced with 0.75 equiv/$\alpha\beta$ of CO under 1 atm of CO_2 (microwave power of 20 mW); D, same as part C except obtained with a microwave power of 0.05 mW; E, ACS reduced with 5 equiv/$\alpha\beta$ of CO under 1 atm of Ar (20 mW); F, same as part E except obtained with a microwave power of 0.05 mW. Pairs of spectra have been corrected for differences in receiver gain and microwave power, such that the displayed intensities at 20 mW would equal those at 0.05 mW if signals were not saturating.

titration can be viewed as an expansion of the most oxidized portion of the MV/CO_2 titration. As BV^{1+} was added, the intensity of the $g_{av} = 1.94$ signal declined and some $g_{av} = 1.82$ signal converted to the $g_{av} = 1.86$ form.[2] The decline of the B_{red} state with added BV^{1+} is consistent with the results of the MV^{1+}/CO_2 and Ti/CO_2 titrations. Taken together, they suggest that $E^{\circ}_{B_{ox}/B_{red}}$ shifted negatively in the presence of these reductants (Ti^{3+} citrate, MV, and BV) under CO_2. No such shift was observed in the presence of CO.

Redox-Dependent Changes in B_{red} Saturation Properties. We have also observed some significant potential-dependent changes in the saturation properties of B_{red}. The B_{red} state saturated in any of the three modes, which is illustrated by the $g_{av} = 1.94$ signals in Figure 7. Spectra B, D, and F were all obtained under nonsaturating conditions (0.05 mW), and their $g_{av} = 1.94$ signals serve as controls. Spectra A, C, and E were obtained from the same samples as those used to obtain spectra B, D, and F, but at 20 mW. Spectrum A, from a reductant-free ACS sample under Ar, illustrates the first saturation mode called Sat1. Sat1 is characterized by a sharp $g = 1.94$ resonance and low-intensity $g = 2.04$ and 1.90 resonances (in Figure 7, the $g = 2.04$, 1.94, and 1.90 resonances occur at 3300, 3470, and 3540 G, respectively). Sat1 has been observed in samples poised at the least negative potentials of our reductive titrations, with the C_{red1} state present. The second saturation mode, illustrated by spectrum C, is called Sat2. Sat2 is characterized by weak intensity from all three resonances. It is associated with CO_2 atmospheres, intermediate potentials (for example, those achieved with BV and MV), and the presence of the C_{red2} and A_{red}−CO states. Sat2 has not been observed for samples prepared under Ar. The third saturation mode, illustrated in spectrum E, is called Sat3. Sat3 is characterized by strong $g = 2.04$, 1.94, and 1.90 resonances with normalized intensities essentially unchanged from that at 0.05 mW. However, the resonances of the Sat3 signal are broader than those of Sat1 under nonsaturating conditions. Sat3 is observed at the most negative potentials of the titrations under an Ar atmosphere with CO or dithionite as a reductant, or under a CO_2 atmosphere using CO, Ti^{3+} citrate, or dithionite as the reductant.

Lindahl et al. interpreted Sat3 as a broad $g_{av} = 1.94$ signal superimposed on a narrower form, arising in samples poised at low potentials (*12*). However, the $g_{av} = 1.94$ signal intensity in spectra from our CO/Ar titration did not increase as it broadened (in ref *11*, compare spectra D and E in Figure 5). Thus, we view this as a change in the saturation properties of B_{red} (from Sat1 to Sat3) rather than as the development of another signal. Development of the A_{red}-CO state seems to be associated with the change in saturation mode.

The situation is somewhat different for the CO/CO_2 titration. In this case, the samples from the more oxidized half of the titration (Figure 1D−F of ref *11*) exhibit Sat2 while those from the more reduced half (Figure 1G,H) exhibit Sat3. The correlation noted above between the A_{red}−CO state and Sat3 is not evident here; rather, A_{red}−CO is present under both Sat2 and Sat3 modes.

A change from Sat1 to Sat2 is illustrated in the MV/CO_2 titration. Spectra E−H of Figure 5 (this paper) show that the $g_{av} = 1.94$ signal intensities were about the same throughout the titration. However, the signals in Figure 5A−C exhibited Sat1, while that in Figure 5D exhibited Sat2. Development of the A_{red}−CO state appears to be associated with this change in saturation. In the MV/Ar titration, B_{red} saturates in the Sat1 mode throughout the titration. In contrast, samples appear to saturate in the Sat3 mode in dithionite/Ar titrations (Figure 1) (*8*). Clearly, further work is required to rationalize these changes. Nevertheless, our studies indicate that B_{red} saturates in three distinct modes, and that the mode that is observed depends on the redox state of the enzyme, the presence or absence of CO_2, and the nature of the reductant. Each saturation mode probably reflects different spatial relationships among the magnetic components in the enzyme, and thus a different enzyme conformation.

DISCUSSION

This paper illustrates the ability of CO_2 and various redox agents to alter the redox, kinetic, and magnetic properties of the metal−sulfur clusters in ACS. Their ability to do this implies that ACS contains binding sites the occupancy of which affects these cluster properties. The enzyme certainly has binding sites for its substrates CO and CO_2, though we cannot exclude the possibility that these molecules elicit their effects by binding to a noncatalytic modulator site on the enzyme (*7*). Some of our results also suggest that the enzyme has binding sites for Ti^{3+}, citrate, MV, and/or BV, though we remain skeptical about this possibility.

The three B_{red} saturation modes described here may reflect three redox- and/or CO_2-dependent conformations of the protein. Mössbauer studies reveal that the B_{red} and C_{red2} states interact magnetically, suggesting that they are separated by ≤15 Å (*10*). In each conformation, the distance and/or orientation of the B_{red} cluster to other clusters in the enzyme may be different.

[2] Two $g_{av} = 1.82$ type signals were present, one with g values of 2.005, 1.84, and 1.68, and the other with g values of 2.005, 1.80, and 1.64. The former has been described earlier for samples prepared under CO_2, while the latter has been observed previously in samples prepared under Ar (*8*). In the BV/CO_2 titration, the CO_2 form disappeared under more oxidizing conditions, suggesting that it has a slightly less negative reduction potential than the Ar form.

Whether these states have catalytic import is uncertain, though those effected by CO_2 may (*14*). Particular states may control the direction of catalysis or facilitate reversibility under various conditions. The enzyme functions under CO_2 in vivo, and is required to reduce CO_2 to CO as part of synthesizing acetyl-CoA. By lowering the potential of the B_{ox}/B_{red} couple and increasing that of the C_{red1}/C_{red2} couple (as observed under CO_2 atmospheres), CO_2 reduction would be favored (B_{red} would be powerful enough to reduce the C-cluster to the C_{red2} state, which could then be used to reduce CO_2). On the other hand, if CO concentrations would become high and CO_2 concentrations low, a lower C_{red1}/C_{red2} potential and higher B_{ox}/B_{red} potential would favor CO oxidation.

We have used these states to stabilize and highlight various states of the enzyme. For example, we can stabilize the C_{red2} state in the near absence of B_{red}. By using phen-treated enzyme (which removes the labile Ni of the A-cluster), samples could be prepared in which the only magnetic state that was present was C_{red2}, and these could be profitably investigated by Mössbauer spectroscopy.

The most important achievement of this paper was the stabilization of the C_{int} state using Ti^{3+} citrate/Ar, for it serves to support the mechanism of catalysis first proposed by Anderson and Lindahl (*8*) and embellished by Hu et al. (*10*) and DeRose et al. (*13*). Earlier studies hinted that the C-cluster could be stabilized in the C_{int} state. Upon addition of CS_2 (an analogue of CO_2) to the reduced enzyme, the $g_{av} = 1.82$ signal disappeared but the $g_{av} = 1.86$ signal did not appear (*8*). A new C-cluster EPR signal (with g values of 1.78, 1.69, and 1.51) slowly developed after the CS_2 treatment. Although some aspects of this experiment remain unexplained (like whether that new signal arose from C_{red2}), we now suggest that the C-cluster was rapidly reduced under these conditions to the C_{int} state. Russell and Lindahl (*14*) also suggested that the C_{int} state formed in their potentiometric CO/CO_2 titrations (the sum of the $g_{av} = 1.82$ and 1.86 signals declined with added reductant), though their results were too subtle to be independently decisive. Seravalli et al. reported the absence of such effects in their stoichiometric titrations (*25*).

The C_{int} state is required because the CO/CO_2 reaction catalyzed at the C-cluster involves donating and/or accepting two electrons in a single step, while electrons transfer into and/or out of the enzyme through the B-cluster in one-electron steps (*8*). ACS employs a mechanism of converting between $n = 2$ and $n = 1$ chemistry and similar to that used by flavins and hydrogenases. The NiFe active site of hydrogenases accepts two electrons from H_2 and apparently passes them on to neighboring Fe−S clusters in one-electron steps. The NiFe active site can be stabilized in three catalytically relevant redox states, including Ni−SI, Ni−C, and Ni−R (*26*, *27*), analogous to C_{red1}, C_{int}, and C_{red2}, respectively. The redox potentials of the analogous couples are similar to those of the C-cluster ($E°_{Ni-SI/Ni-C} = -0.330$ V and $E°_{Ni-C/Ni-R} = -0.405$ V at pH 8). This is not surprising, for the $E°'$ value of the reactions catalyzed at that site is similar to that catalyzed at the C-cluster ($E°_{CO/CO_2} = -0.512$ V and $E°_{H_2/H^+} = -0.413$ V at pH 7) (*28*). Both Ni−Fe−S clusters also stabilize a more oxidized noncatalytically relevant state (C_{ox} and Ni−AB). One difference is in spin states; the intermediate (Ni−C) state has an S of $^1/_2$ and exhibits a well-studied EPR signal, while Ni−SI and Ni−R are both EPR-silent. Given the similar catalytic properties and metal−sulfur composition, it would be interesting to compare the atomic level structures of the two active sites.

ACKNOWLEDGMENT

We thank William K. Russell and David P. Barondeau for preliminary helpful studies using Ti/Ar. We also thank a reviewer of this paper for suggesting that we examine the kinetics of the Ti^{3+} citrate effect.

REFERENCES

1. Ragsdale, S. W., and Kumar, M. (1996) *Chem. Rev. 96*, 2515−2539.
2. Ferry, J. G. (1995) *Annu. Rev. Microbiol. 49*, 305−333.
3. Dai, Y.-R., Reed, D. W., Millstein, J. H., Hartzell, R. L., Grahame, D. A., and DeMoll, E. (1998) *Arch. Microbiol. 169*, 525−529.
4. Kerby, R. L., Ludden, P. W., and Roberts, G. P. (1995) *J. Bacteriol. 177*, 2241−2244.
5. Anderson, M. E., DeRose, V. J., Hoffman, B. M., and Lindahl, P. A. (1993) *J. Am. Chem. Soc. 115*, 12204−12205.
6. Kumar, M., Lu, W.-P., Liu, L., and Ragsdale, S. W. (1993) *J. Am. Chem. Soc. 115*, 11646−11647.
7. Anderson, M. E., and Lindahl, P. A. (1994) *Biochemistry 33*, 8702−8711.
8. Anderson, M. E., and Lindahl, P. A. (1996) *Biochemistry 35*, 8371−8380.
9. Lindahl, P. A., Ragsdale, S. W., and Münck, E. (1990) *J. Biol. Chem. 265*, 3880−3888.
10. Hu, Z., Spangler, N. J., Anderson, M. E., Xia, J., Ludden, P. W., Lindahl, P. A., and Münck, E. (1996) *J. Am. Chem. Soc. 118*, 830−845.
11. Fraser, D. M., and Lindahl, P. A. (1999) *Biochemistry 38*, 15697−15705.
12. Lindahl, P. A., Münck, E., and Ragsdale, S. W. (1990) *J. Biol. Chem. 265*, 3873−3880.
13. DeRose, V. J., Telser, J., Anderson, M. E., Lindahl, P. A., and Hoffman, B. M. (1998) *J. Am. Chem. Soc. 120*, 8767−8776.
14. Russell, W. K., and Lindahl, P. A. (1998) *Biochemistry 37*, 10016−10026.
15. Shin, W., and Lindahl, P. A. (1993) *Biochim. Biophys. Acta 1161*, 317−322.
16. Pelley, J. W., Garner, C. W., and Little, G. H. (1978) *Anal. Biochem. 86*, 341−343.
17. Morton, T. A., Rundquist, A. R., Ragsdale, S. W., Shanmugasundaram, T., Wood, H. G., and Ljundahl, L. G. (1991) *J. Biol. Chem. 266*, 23824−23828.
18. Shin, W., Stafford, P. R., and Lindahl, P. A. (1992) *Biochemistry 31*, 6003−6011.
19. Orme-Johnson, N. R., and Orme-Johnson, W. H. (1978) *Methods Enzymol. 52*, 252−257.
20. Zehnder, A. J. B., and Wuhrmann, K. (1976) *Science 194*, 1165−1166.
21. Shin, W., and Lindahl, P. A. (1992) *Biochemistry 31*, 12870−12875.
22. Sawyer, D. T., and Roberts, J. L. (1974) *Experimental Electrochemistry for Chemists*, John Wiley & Sons, New York.
23. Fultz, M. L., and Durst, R. (1982) *Anal. Chim. Acta 140*, 1−18.
24. Szentrimay, R., Yeh, R., and Kuwana, T. (1977) in *Electrochemical Studies of Biological Systems* (Sawyer, D. T., Ed.) pp 142−169, ACS Symposium Series 38, American Chemical Society, Washington, DC.
25. Seravalli, J., Kumar, M., Lu, W.-P., and Ragsdale, S. W. (1997) *Biochemistry 36*, 11241−11251.
26. Roberts, L. M., and Lindahl, P. A. (1994) *Biochemistry 33*, 14339−14350.
27. Roberts, L. M., and Lindahl, P. A. (1995) *J. Am. Chem. Soc. 117*, 2565−2572.
28. Reiger, P. H. (1994) *Electrochemistry*, Chapman & Hall, New York.

BI990398F